Nonlinear magneto-optical resonances at D_1 excitation of ^{85}Rb and ^{87}Rb in an extremely thin cell

M. Auzinsh[1],* R. Ferber[1], F. Gahbauer[1], A. Jarmola[1], L. Kalvans[1], A. Papoyan[2], and D. Sarkisyan[2]
[1]*Laser Centre, The University of Latvia, 19 Rainis Boulevard, LV-1586 Riga, Latvia*
[2]*Institute for Physical Research, NAS of Armenia, Ashtarak-0203, Armenia*
(Dated: September 28, 2009)

Nonlinear magneto-optical resonances have been measured in an extremely thin cell (ETC) for the D_1 transition of rubidium in an atomic vapor of natural isotopic composition. All hyperfine transitions of both isotopes have been studied for a wide range of laser power densities, laser detunings, and ETC wall separations. Dark resonances in the laser induced fluorescence (LIF) were observed as expected when the ground state total angular momentum F_g was greater than or equal to the excited state total angular momentum F_e. Unlike the case of ordinary cells, the width and contrast of dark resonances formed in the ETC dramatically depended on the detuning of the laser from the exact atomic transition. A theoretical model based on the optical Bloch equations was applied to calculate the shapes of the resonance curves. The model averaged over the contributions from different atomic velocity groups, considered all neighboring hyperfine transitions, took into account the splitting and mixing of magnetic sublevels in an external magnetic field, and included a detailed treatment of the coherence properties of the laser radiation. Such a theoretical approach had successfully described nonlinear magneto-optical resonances in ordinary vapor cells. Although the values of certain model parameters in the ETC differed significantly from the case of ordinary cells, the same physical processes were used to model both cases. However, to describe the resonances in the ETC, key parameters such as the transit relaxation rate and Doppler width had to be modified in accordance with the ETC's unique features. Agreement between the measured and calculated resonance curves was satisfactory for the ETC, though not as good as in the case of ordinary cells.

PACS numbers: 32.60.+i,32.80.Xx,32.10.Fn

I. INTRODUCTION

Atomic vapors confined between walls separated by only a few hundred nanometers have the potential for interesting applications in magnetometry and optoelectronics [1, 2]. Spectroscopic cells that have two walls separated by a distance that is on the order of the wavelength of visible or near infra-red light are known as extremely thin cells (ETCs) [3]. If the laser radiation propagates in a direction perpendicular to the ETC walls, fluorescence will be observed preferentially from those atoms whose velocity vectors have a small normal component with respect to the walls, since atoms flying rapidly towards an ETC wall will collide with it before being able to fluoresce. As a result, sub-Doppler spectroscopic resolution can be achieved in an ETC [3]. This useful feature can be exploited to study physical phenomena in atomic systems with hyperfine manifolds that are not resolved under normal conditions, such as resonances at zero magnetic field in a plot of laser induced fluorescence (LIF) versus magnetic field. These resonances can be dark [4, 5] or bright [6]. They arise when at zero magnetic field the ground state magnetic sublevels form a quantum superposition state, which is not coupled to the exciting laser field in the case of dark resonances, but coupled strongly in the case of bright resonances. Although the theoretical description of these resonances is straightforward in principle, the theoretical calculations have failed at times to reproduce accurately the experimental signals, in part, because in most available systems the excited state hyperfine levels were not resolved under Doppler broadening. The development of the ETC offered a way to address this issue, because the ETC makes possible sub-Doppler resolution. This approach was taken by Andreeva and co-workers [7] for the case of cesium. However, the results contained some surprises in that some resonances that would be bright in an ordinary cell appeared dark in the ETC.

The goal of the present study was to obtain experimental resonance signals with an ETC for the rubidium D_1 transition with high accuracy and as a function of several well-defined parameters. Then, we planned to apply to these data a theoretical model that had been developed to describe nonlinear magneto-optical resonances in ordinary vapor cells [8, 9], to see if we could obtain an adequate theoretical description of bright and dark resonances in ETCs with this model.

Nonlinear magneto-optical resonances are closely related to the ground state Hanle effect, which was first observed by Lehmann and Cohen-Tannoudji in 1964 [10]. Schmieder [5] and later Alzetta [4] observed dark resonances in alkali atoms. In 1978, Piqué successfully applied a theoretical model based on the optical Bloch equations to describe measurements of dark resonances in the $F_g = 2 \rightarrow F_e = 1$ transition of the D_1 line in a beam of sodium atoms [11]. In 2000, Dancheva et al. [6] observed bright resonances for the first time in the D_1 and D_2 transitions of rubidium in an atomic vapor. Papoyan et

*Electronic address: Marcis.Auzins@lu.lv

al. [12] applied a theoretical model [13] based on the optical Bloch equations to bright and dark resonances in the D_2 transition of cesium observed in a vapor cell. However, their calculations predicted a bright resonance for the $F_g = 4 \rightarrow F_e = 3, 4, 5$ transition, whereas for linearly polarized excitation it appeared to be dark in the experiment. Andreeva et al. [7] studied bright and dark resonances in ETCs and suggested that spin-changing collisions of the atoms with the walls could change some bright resonances into dark resonances.

Our initial approach to the difficulties in describing bright and dark resonances in atomic vapors was to develop further a theoretical model [13] so that it that would take into account the Doppler effect. Besides averaging over the Doppler profile, the model also accounted for all nearby hyperfine transitions, the splitting and mixing of the magnetic sublevels in the magnetic field, and the coherence properties of the laser radiation. We applied such a model first to the cesium D_1 transition [8], which is almost resolved under Doppler broadening, and then to the rubidium D_1 transition [9], which is partially resolved. The model was successful in describing experimentally measured resonances in ordinary cells for a wide variety of laser power densities, beam diameters, and laser frequency detunings. It required only a few parameters to be adjusted. These parameters were the conversion between the Rabi frequency and the laser power density, the conversion between the laser beam diameter and the transit relaxation time, and the percentage of background from scattered laser-induced fluorescence (LIF). Once the parameters were determined, the same values were used for all data sets. This model served as the starting point of our efforts to describe bright and dark resonances in the ETC.

The level scheme of the D_1 line in ^{85}Rb and ^{87}Rb is shown in Fig. 1. The allowed transitions between the ground and excited states are represented by the arrows with the relative transition strengths given by the fractions next to the arrows. The energy difference between the excited state hyperfine levels is 361.6 MHz for ^{85}Rb [14] and 814.5 MHz for ^{87}Rb [15]. In an ordinary vapor cell, the full width at half maximum (FWHM) of the Doppler broadening for the rubidium D_1 transition at room temperature would be about 500 MHz. In the ETC, however, the Doppler broadening is reduced, because atoms flying parallel to the walls are more likely to be observed in the experiment. The LIF excitation spectra of the D_1 line of natural rubidium for both an ordinary vapor cell and an ETC are shown in Fig. 2. In the ordinary cell, the two excited state hyperfine levels of ^{87}Rb are almost resolved under Doppler broadening, but the hyperfine levels of ^{85}Rb are practically unresolved. In the ETC, however, each transition can be resolved easily.

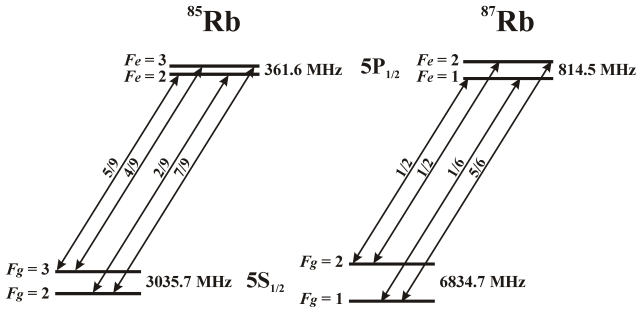

FIG. 1: Hyperfine level structure and transitions of the D_1 line of rubidium. The fractions on the arrows indicate the relative transition strengths [14, 15].

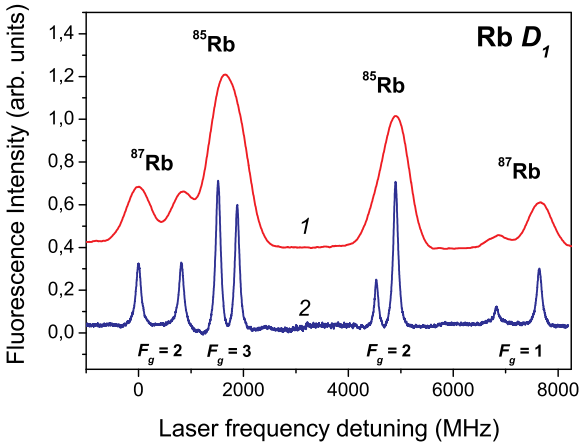

FIG. 2: (color online) LIF excitation spectra of the Rb D_1 line. Curve 1: in an ordinary cell at 10 mW/cm^2 excitation; curve 2: in an ETC at 10 mW/cm^2 excitation and wall separation $L = \lambda/2$, where λ is the wavelength of the laser radiation.

II. EXPERIMENT

The ETC was produced at the Institute of Physical Research in Ashtarak, Armenia, while the experiments described here were performed in Riga. The principle of the ETC is described in [1, 3]. Basically, it consists of two YAG crystals that are sealed in such a way that the separation between the two crystals varies from 50 nm to about 1.8 μm. Rubidium metal is stored in a glass arm that is bonded to the YAG crystals. The cell was operated in a two-chambered oven, which keeps the YAG windows at about 200^{o}C and the rubidium arm at about 150^{o}C. The laser was a DL 100 external cavity single mode diode laser with a wavelength of 794.3 nm and a typical line width of a few megahertz, which was produced by Toptica, A. G., of Graefelfing, Germany. The laser beam passed through a Glan-Thompson polarizer before entering the cell. The cell was placed at the cen-

ter of a three-axis Helmholtz coil system, which rested on a nonmagnetic optical table. Two pairs of coils compensated the laboratory magnetic field, while the third pair of coils was used to scan the magnetic field in the observation direction. The current in this third pair of coils was scanned with a Kepco BOP-50-8M bipolar power supply, which was controlled by an analog signal from a computer. Figure 3 depicts the relative orientation of the laser beam (exc), the laser radiation's linear polarization vector ($\mathbf{E}_{exc}$), the magnetic field ($\mathbf{B}$), the observation direction (obs), and the ETC walls. The experimental setup and auxiliary equipment were similar to what was used in [8]. Data was acquired with a National Instruments 6024E data acquisition card.

The laser induced fluorescence was detected by means of a Thorlabs FDS-100 photodiode as a function of magnetic field for all hyperfine transitions of the two isotopes of rubidium (see Fig. 1). Fluorescence emerged through the side walls of the ETC, which means that the detected fluorescence may have undergone various reflections inside the ETC and been scattered while traversing the glue that seals the ETC walls. No polarizers were used in the LIF observation. Signals were obtained for various laser power densities between 10 mW/cm^2 and 2000 mW/cm^2. The laser beam diameter was usually 0.44 mm (FWHM of intensity), as measured by a Thorlabs BP 104-VIS beam profiler, but different laser beam diameters were also applied to the cell.

To record the signal, the laser's frequency was maintained at the value that gave the maximum fluorescence signal at a given transition. The fluorescence was recorded while the magnetic field was scanned several times, and the scans were averaged. The laser was not actively stabilized, but its frequency was monitored with a High Finesse WS-7 wavemeter. Scans for which the contrast deviated significantly from the average as a result of laser frequency drift were eliminated from the average. For some observations we used a double scanning technique [16], in which the laser frequency was scanned slowly across a transition while the magnetic field was scanned more rapidly from negative to positive values with a triangular waveform. The laser frequency changed by about 2–5 MHz per second. The typical laser frequency scan lasted about 1–2 minutes, whereas the typical period for the magnetic field scan was 1 second. In this manner, a series of resonance signals at laser frequencies differing by 2–5 MHz could be obtained.

In addition to the signal, each measurement included a certain amount of background. Background from scattered laser light was determined for each measurement by tuning the laser off resonance. However, there was an additional background associated with scattered LIF, which could not be readily identified. Studies in the ordinary cell had suggested that this background accounts for a fixed percentage of the signal for a given vapor cell. The value of this background was one of the parameters that had to be adjusted to find the best fit between experiment and theory for the entire data set.

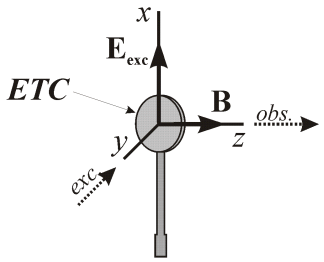

FIG. 3: Experimental geometry. The relative orientation of the laser beam (exc), laser light polarization ($\mathbf{E}_{exc}$), magnetic field ($\mathbf{B}$), observation direction (obs), and ETC walls are shown.

A typical dark resonance in the ETC is shown in the inset of Fig. 4, which also shows the dependence of the FWHM and contrast of the resonances versus the inverse of a characteristic length that characterizes the interaction of the atoms with the laser radiation. This characteristic length will be described in the next section.

III. THEORY

A theoretical model had been developed previously in order to describe bright and dark resonances in ordinary vapor cells [8, 9]. One of the parameters that determined the width and contrast of the resonances in the theoretical description of ordinary vapor cells was a transit relaxation rate γ, which is the rate at which atoms fly out of the region of interaction with the laser radiation. This transit relaxation rate thus is related to the laser beam diameter. The solid squares in Fig. 4 mark the dependence of the resonance width and contrast on the inverse square root of the cross-sectional area S of the beam, which is related to the inverse of the laser beam diameter in the ordinary cell. In the ETC, resonances are significantly broader than in ordinary cells, and their contrast is much smaller. The question arises, are the resonance width and contrast in the ETC still controlled by a transit relaxation rate γ, and if so, what is the length corresponding to this transit relaxation rate? In our experiments the laser beam diameter was much larger than the ETC wall separation; thus the characteristic length in the ETC should be related to the wall separation rather than to the laser beam diameter. However, a Voigt profile fit to the fluorescence peaks in an LIF excitation spectrum of the ETC (similar to curve 2 in Fig. 2) revealed that the Doppler width in the ETC is approximately 60 MHz (FWHM) when the wall separation L is equal to the wavelength λ of the laser radiation. The Doppler width corresponding to that temperature in an ordinary cell would be about ten times greater. One could therefore say that a typical atom that fluoresces and travels at the average thermal speed, flies on a trajectory that makes an angle with respect to the ETC wall such that the flight path between the walls is about ten times the

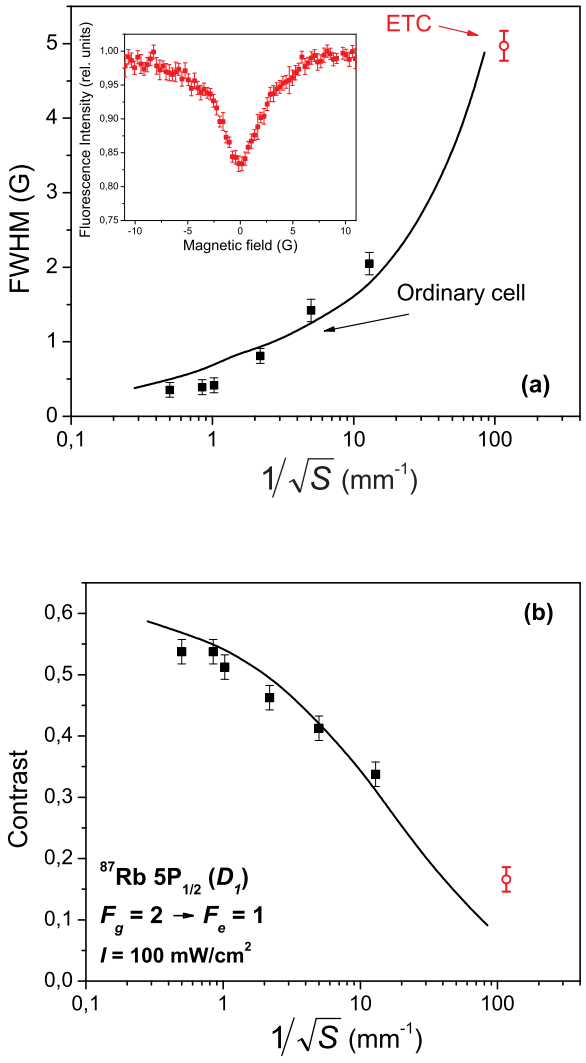

FIG. 4: (color online) Resonance (a) width and (b) contrast as a function of the inverse size of the interaction region with the beam: the square root of the cross-sectional area of the beam in the case of the ordinary cell [9] and the characteristic length before collision in case of the ETC. Filled squares—experiment in an ordinary cell; open circles: experiment in an ETC; solid curve: theory. The inset in (a) shows a typical dark resonance in the ETC. Data are for the $F_g = 2 \rightarrow F_e = 1$ transition of ^{87} Rb at a laser power density of 100 mW/cm^2.

wall separation. Indeed, the abscissa of the open circles in Fig. 4, which correspond to the resonance width and contrast in the ETC, have been chosen to correspond to a length dimension that is about ten times the wall separation, and the circles lie rather close to the extrapolation of the theoretical model developed for ordinary cells. Strictly speaking, it is not correct to extend the theoretical calculation with the parameter values chosen for ordinary cells into the regime of the ETC. However, Fig. 4 suggested that a single theoretical approach might be able to describe qualitatively the width and contrast of nonlinear magneto-optical resonances in alkali vapors over several orders of magnitude of a single dimension, which is related to a transit relaxation rate γ. Hence, we formulated the hypothesis that the shapes of nonlinear magneto-optical resonances in an ETC can be described by the same model that describes these signals in ordinary cells when the particular characteristics of the ETC are reflected in appropriately chosen values of the model parameters.

A detailed description of this theoretical model can be found in [8, 9]. The model describes the internal atomic dynamics by a semi-classical atomic density matrix ρ, which also depends parametrically on the classical coordinates of the atomic center of mass. The time evolution of the density matrix ρ follows the optical Bloch equations (OBEs) [17]:

$$i\hbar\frac{\partial\rho}{\partial t} = \left[\hat{H},\rho\right] + i\hbar\hat{R}\rho. \qquad (1)$$

The relaxation operator $\hat{R}$ includes the spontaneous emission rate, which equals the natural transition linewidth Γ, and the transit relaxation rate γ, which in the case of the ETC corresponds to the rate of collisions with the cell wall. The Hamiltonian $\hat{H}$ is given by $\hat{H} = \hat{H}_0 + \hat{H}_B + \hat{V}$. $\hat{H}_0$ is the unperturbed atomic Hamiltonian and depends on the internal atomic coordinates, $\hat{H}_B$ is the Hamiltonian of the atomic interaction with the magnetic field, and $\hat{V} = -\hat{\mathbf{d}}\cdot\mathbf{E}(t)$ is the dipole interaction operator.

Taking into account the classical motion of the atoms and the resulting Doppler shifts, we apply the rotating wave approximation [18] to the OBEs. This approximation yields stochastic differential equations, which can be further simplified by using the decorrelation approach [19]. Since the experimentally observed light intensity is averaged over time intervals that are large compared to the characteristic time of the phase fluctuations, it is permissible to average over the stochastic differential equations following the method described in [13].

After eliminating the density matrix elements that correspond to optical coherences, we arrive at the equations

for the Zeeman coherences:

$$\frac{\partial\rho_{g_ig_j}}{\partial t} = \big(\Gamma_{p,g_ie_m} + \Gamma^*_{p,e_kg_j}\big)\sum_{e_k,e_m}\big(d_1^{g_ie_k}\big)^* d_1^{e_mg_j}\rho_{e_ke_m} - \sum_{e_k,g_m}\Big[\Gamma^*_{p,e_kg_j}\big(d_1^{g_ie_k}\big)^* d_1^{e_kg_m}\rho_{g_mg_j} + \Gamma_{p,g_ie_k}\big(d_1^{g_me_k}\big)^* d_1^{e_kg_j}\rho_{g_ig_m}\Big] - i\omega_{g_ig_j}\rho_{g_ig_j} + \sum_{e_i,e_j}\Gamma^{e_ie_j}_{g_ig_j}\rho_{e_ie_j} - \gamma\rho_{g_ig_j} + \lambda\delta\big(g_i,g_j\big) \qquad (2)$$

and

$$\frac{\partial\rho_{e_ie_j}}{\partial t} = \big(\Gamma^*_{p,e_ig_m} + \Gamma_{p,g_ke_j}\big)\sum_{g_k,g_m} d_1^{e_ig_k}\big(d_1^{g_me_j}\big)^*\rho_{g_kg_m} - \sum_{g_k,e_m}\Big[\Gamma_{p,g_ke_j}d_1^{e_ig_k}\big(d_1^{g_ke_m}\big)^*\rho_{e_me_j} + \Gamma^*_{p,e_ig_k}d_1^{e_mg_k}\big(d_1^{g_ke_j}\big)^*\rho_{e_ie_m}\Big] - i\omega_{e_ie_j}\rho_{e_ie_j} - \Gamma\rho_{e_ie_j}. \qquad (3)$$

In these equations $\rho_{g_ig_j}$ and $\rho_{e_ie_j}$ are the density matrix elements for the ground and excited states, respectively. The first term in (2) describes the re-population of the ground state and the creation of Zeeman coherences from induced transitions; Γ_{p,g_ie_j} and Γ^*_{p,e_ig_j} are the couplings between the laser field and the ground and excited states; and $d_1^{e_ig_j}$ is the dipole transition matrix element between the ground state i and the excited state j. The second term contains the changes of the ground state Zeeman sublevel population and the creation of ground state Zeeman coherences after light absorption. The third term describes the destruction of the ground state Zeeman coherences by the external magnetic field; $\omega_{g_ig_j}$ is the splitting of the ground state Zeeman sublevels. The fourth term describes the re-population and transfer of excited state coherences to the ground state as a result of spontaneous transitions. We assume our transition to be closed (within the fine structure, all atoms undergoing spontaneous transitions return to the initial fine structure state $5S_{1/2}$), and so $\sum_{e_i,e_j}\Gamma^{e_ie_j}_{g_ig_j} = \Gamma$. The fifth and sixth terms show the relaxation and re-population of the ground state due to non-optical reasons; in our case it is assumed to be solely transit relaxation. We assumed that the atomic equilibrium density outside the interaction region is normalized to 1, and so $\lambda = \gamma$.

In equation (3) the first term describes the light absorbing transitions; the second term denotes induced transitions to the ground state; the third describes the destruction of ground state Zeeman coherences in the external magnetic field, where $\omega_{e_ie_j}$ is the splitting of the excited state Zeeman sublevels; and the fourth term denotes the rate of spontaneous decay of the excited state.

The interaction strength Γ_{p,g_ie_j} is given by

$$\Gamma_{p,g_ie_j} = \frac{|\varepsilon_{\overline{\omega}}|^2}{\hbar^2}\frac{1}{\big[\big(\frac{\Gamma}{2}+\frac{\Delta\omega}{2}\big) \pm i\left(\overline{\omega} - \boldsymbol{k}_{\overline{\omega}}\boldsymbol{v} - \omega_{e_jg_i}\right)\big]}, \qquad (4)$$

where $|\varepsilon_{\overline{\omega}|^2}/\hbar^2$ is proportional to the laser power density.

The magnetic field not only splits the Zeeman sublevels by an amount ω_{ij}, but also changes the transition dipole elements by mixing the magnetic sublevels. The Breit-Rabi formula [20, 21] gives the mixing in the case of two hyperfine levels. Although the ground state hyperfine levels are separated by several gigahertz, all four hyperfine components were taken into account simultaneously for modeling the experimental signals. As can be seen from equation (4), absorption is possible from both hyperfine levels in one experiment, even when taking into account the natural linewidth of the optical transition, the Doppler lineshift, and the laser detuning from the exact resonance.

The experiments took place under stationary excitation conditions so that $\partial\rho_{g_ig_j}/\partial t = \partial\rho_{e_ie_j}/\partial t = 0$. Thus, one can reduce the differential equations (2) + (3) to a system of linear equations and solve it to obtain the density matrices for the atomic ground and excited states. From the density matrices, one obtains the observed fluorescence intensity as follows:

$$I_f(\tilde{\mathbf{e}}) = \tilde{I}_0\sum_{g_i,e_i,e_j} d^{(ob)*}_{g_ie_j}d^{(ob)}_{g_ie_i}\rho_{e_ie_j}, \qquad (5)$$

where $\tilde{I}_0$ is a constant of proportionality.

The signal is summed over the different atomic velocity groups, over the two orthogonal polarization components of the fluorescence, and over all nearby hyperfine transitions, including both ground state hyperfine levels.

Among the adjustable parameters of the model are the conversion between laser power density I and Rabi frequency Ω_R, the conversion between the ETC wall separation and the transit relaxation rate γ, and the Doppler width, which was different in the ETC from the case of the ordinary cell. Atomic constants are taken from the compilation by Steck [14, 15].

IV. RESULTS AND DISCUSSION

In general, one expects to observe dark resonances if the total ground state momentum F_g is greater than or equal to the total excited state momentum F_e and a bright resonance if $F_g < F_e$ [22, 23, 24]. Figures 5 and 6 show magneto-optical resonances for the various hyperfine transitions at the D_1 line of ^{87}Rb and ^{85}Rb, respectively. Dark resonances were clearly seen as expected at the $F_g = 2 \rightarrow F_e = 1$, $F_g = 2 \rightarrow F_e = 2$, and $F_g = 1 \rightarrow F_e = 1$ transitions shown in Fig. 5, and at the $F_g = 3 \rightarrow F_e = 2$, $F_g = 3 \rightarrow F_e = 3$, and $F_g = 2 \rightarrow F_e = 2$ transitions shown in Fig. 6, since $F_g \geq F_e$. However, neither the $F_g = 1 \rightarrow F_e = 2$ transition in ^{87}Rb nor the $F_g = 2 \rightarrow F_e = 3$ transition in ^{85}Rb gave any indication of either a bright or dark resonance associated with ground state coherences, even though one might have expected a bright resonance here since $F_g < F_e$. We note, however, that the theoretical calculations also did not show a bright resonance.

The decrease of the observed fluorescence with increasing magnetic field was related to the fact that at high magnetic fields the energy separation of individual transitions between the Zeeman sublevels exceeded the laser linewidth, and hence resonant absorption was reduced. The reason that no bright resonance could be observed was probably that, compared to the ordinary cell, the resonances in the ETC were much broader and their contrast was much reduced. In the ordinary cell, the contrast of the bright resonance at the $F_g = 1 \rightarrow F_e = 2$ transition of ^{87}Rb was a mere 0.15%. In the ETC, it was too small to observe at our experimental sensitivity. Bright resonance contrast rapidly decreases when one goes from a closed to a partially open transition, which is the case with respect to the hyperfine structure in this system, although for ordinary cells it is still barely observable.

It has been shown previously in an ordinary rubidium vapor cell that the shape of a nonlinear magneto-optical resonance is sensitive to detuning [9]. The ETC should be much more sensitive to detuning because of its sub-Doppler characteristics. Figure 7 depicts the $F_g = 3 \rightarrow F_e = 2$ transition of ^{85}Rb for various values of the detuning from the point of maximum fluorescence between 0 and 15 MHz. As in the case of the ordinary cell, the contrast decreased as the laser was detuned from the resonance, but in the ETC the effect was much more dramatic. In the ETC, a detuning of only 20 MHz resulted in a reduction in the contrast of the dark resonance that was comparable to the reduction observed in the ordinary cell for a detuning of 300 MHz [9] at the $F_g = 3 \rightarrow F_e = 2$ transition of ^{85}Rb.

Among the parameters that one must know in order to fit the resonance shapes is the Rabi frequency Ω, which is related to the laser power density I as $I = k_{Rabi}\Omega^2$. This parameter was one of the ones that had to be adjusted in order to find the best fit for all the data obtained over all transitions of both isotopes at various powers. Figure 8 shows the $F_g = 1 \rightarrow F_e = 1$ transition of ^{87}Rb at various laser power densities. The filled squares show the results of the experiment, whereas the solid line shows the result of the theoretical calculation. Similar to the case of the ordinary cell, the resonance contrast and width increased with increasing Rabi frequency, but the increase leveled off at higher Rabi frequencies. Figure 9 shows the measured and calculated resonance contrast for all dark resonances of the rubidium D_1 transition.

The model assumed a residual Doppler width in the direction transverse to the ETC walls on order of 60 MHz (FWHM) for all calculations corresponding to $L = \lambda$. This Doppler width corresponds to the value obtained by fitting a Voigt profile to the LIF excitation spectrum for wall separation $L = \lambda$. The Doppler width in the direction transverse to the ETC walls was therefore about ten times less than the Doppler width in the directions parallel to the walls at the ETC temperature.

The value of the transit relaxation rate γ was 1.4 MHz, and it was the same for all theoretical calculations corresponding to ETC wall separation $L = \lambda$. In an ordinary cell, such a transit relaxation rate would correspond to a beam diameter about twenty times the value of the ETC wall separation. Although from the decrease in Doppler width this factor might have been expected to be ten rather than twenty, the distribution of transit times for atoms that are traversing a cylindrical laser beam in an ordinary cell differs from the corresponding distribution for atoms that are flying between two parallel walls in an ETC.

Since the ETC cell walls are inclined toward each other, it is possible to perform the experiment at different wall separations. Both the residual Doppler width and the transit relaxation time γ^{-1} should depend linearly on the ETC wall separation. The approximate wall separation L can be inferred from the constructive ($L = (2n+1)\lambda/4$) or destructive ($L = n\lambda/2$) interference of the laser beams of wavelength λ reflected from the ETC's two inside walls. Figure 10 shows the laser induced fluorescence intensity versus the magnetic field for $L = \lambda/2$, $L = 3\lambda/4$, $L = \lambda$, and $L = 3\lambda/2$. The theoretical curves are calculated with residual Doppler width and transit relaxation time linearly proportional to the wall separation, and they follow the trend of the experimentally measured curves.

Other parameters included were 10 MHz for the laser line width as well as the atomic parameters from [14, 15]. The background from scattered LIF was also adjusted by seeking the best fit to all the data. It was taken to be 50% for all transitions of ^{87}Rb and ^{85}Rb. The reason for such a high background from scattered LIF was that the fluorescence observed by the detector might have been reflected by the walls of the ETC or scattered while passing through the glue that held the walls together (see Fig. 3).

In general the agreement between the experimental data and the calculations was satisfactory over a wide range of different experimental conditions and for four distinct hyperfine transitions in each of two isotopes, though it was not nearly as good as was the case for the ordinary cell [9]. There are several reasons why agreement between experiment and calculations in the ETC should not have been as good as was the case for the ordinary cell. For one thing, the ETC cell thickness is a rapidly changing and nonlinear function of position. The neutral density filters used to obtain different laser power densities could displace the laser beam slightly to an area with a different cell thickness and hence relaxation time γ^{-1}. Furthermore, the laser beam was about 0.4 mm in diameter, and so the ETC thickness was not constant within the laser beam. Also, the resonances in the ETC were much more sensitive to laser detuning (see Fig. 7) than in the ordinary cell. Thus, the inevitable small drift of the laser frequency during a single measurement or between measurements, which had negligible impact on the results in the ordinary cell, had a greater impact on the results of the ETC. On the other hand, the model was able to describe the data in the ETC at higher laser power densities, because in the ETC, which has a larger transit relaxation rate, the saturation parameter Ω^2/Γ_γ is smaller than in the ordinary cell for the same Ω^2.

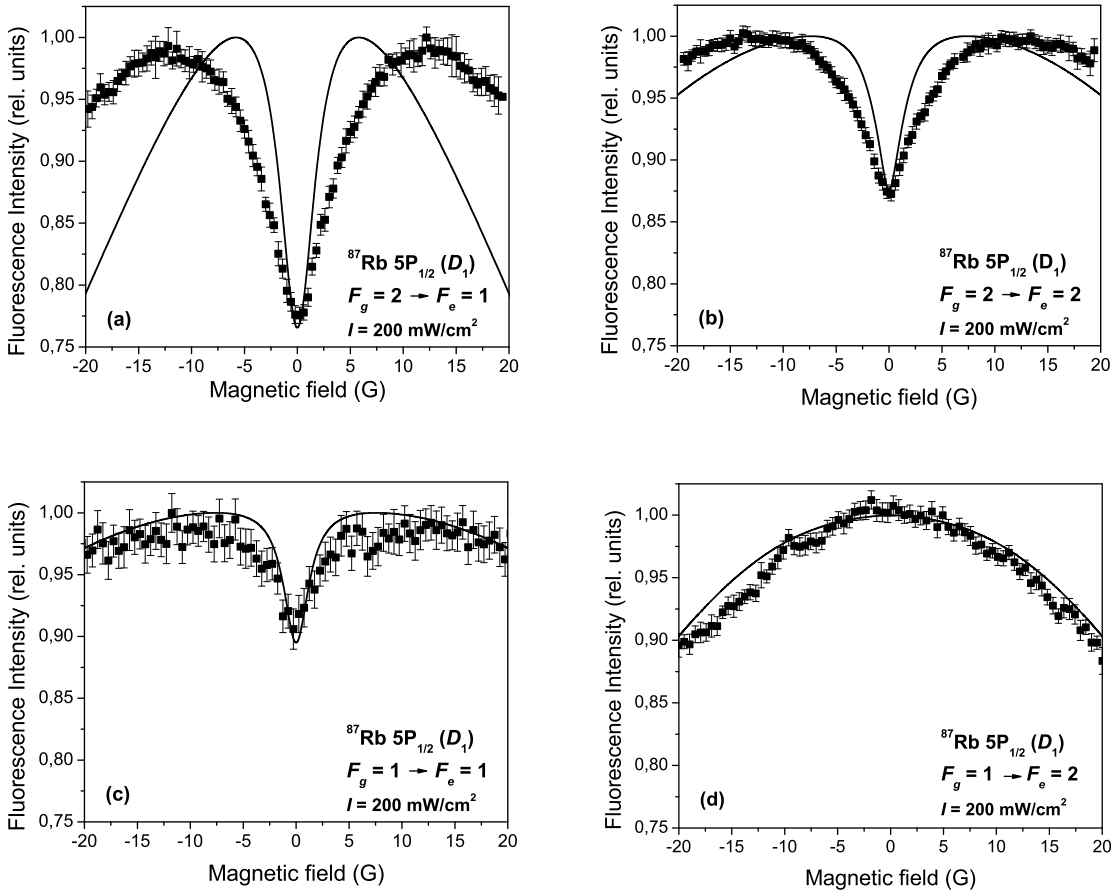

FIG. 5: Fluorescence intensity versus magnetic field for ^{87}Rb at D_1 excitation. Filled squares, experiment; solid line, theory. The excited state, total angular momentum of the ground F_g and excited states F_e of the transition and laser power density I are given in each panel. Wall separation $L = \lambda$, the wavelength of the light.

It should be noted that the experimental dependence on the frequency detuning Δ of the width and contrast of the dark resonances formed in the ETC (Fig. 7) were in agreement with the results of the dark resonance formation in an ETC in a Λ-system with two lasers (^{85}Rb $5S_{1/2}$,$F_g = 2 \rightarrow 5P_{3/2} \rightarrow 5S_{1/2}$,$F_g = 3$) [25, 26]. Namely, as the coupling laser was detuned from the resonance with an atomic transition, a strong increase of the resonance width of the electromagnetically induced transparency and a worsening of the contrast were recorded. In ordinary cm–size cells, effectively the opposite behavior would be observable.

When the coupling laser frequency was in exact resonance with corresponding atomic transition in the above mentioned case of the formation of dark resonances in a Λ-system in an ETC, a weak dependence of the dark resonance width on L (as $\sim 1/L^{1/4}$) was observed [1]. The dependence of linewidth on L presented in Fig. 10 was somewhat stronger. This could have been caused by a rapid increase of the width of the dark resonance ($\sim 1/L$) as the thickness decreased for the case of large Δ [1].

V. CONCLUSION

Nonlinear magneto-optical resonances have been measured for all hyperfine transitions of the D_1 line of ^{85}Rb and ^{87}Rb in an ETC under a wide variety of experimental conditions, which included different laser power densities, laser detunings, and ETC thicknesses. Dark resonances have been observed as expected for all hyperfine transitions with $F_g \geq F_e$. Bright resonances were not observed

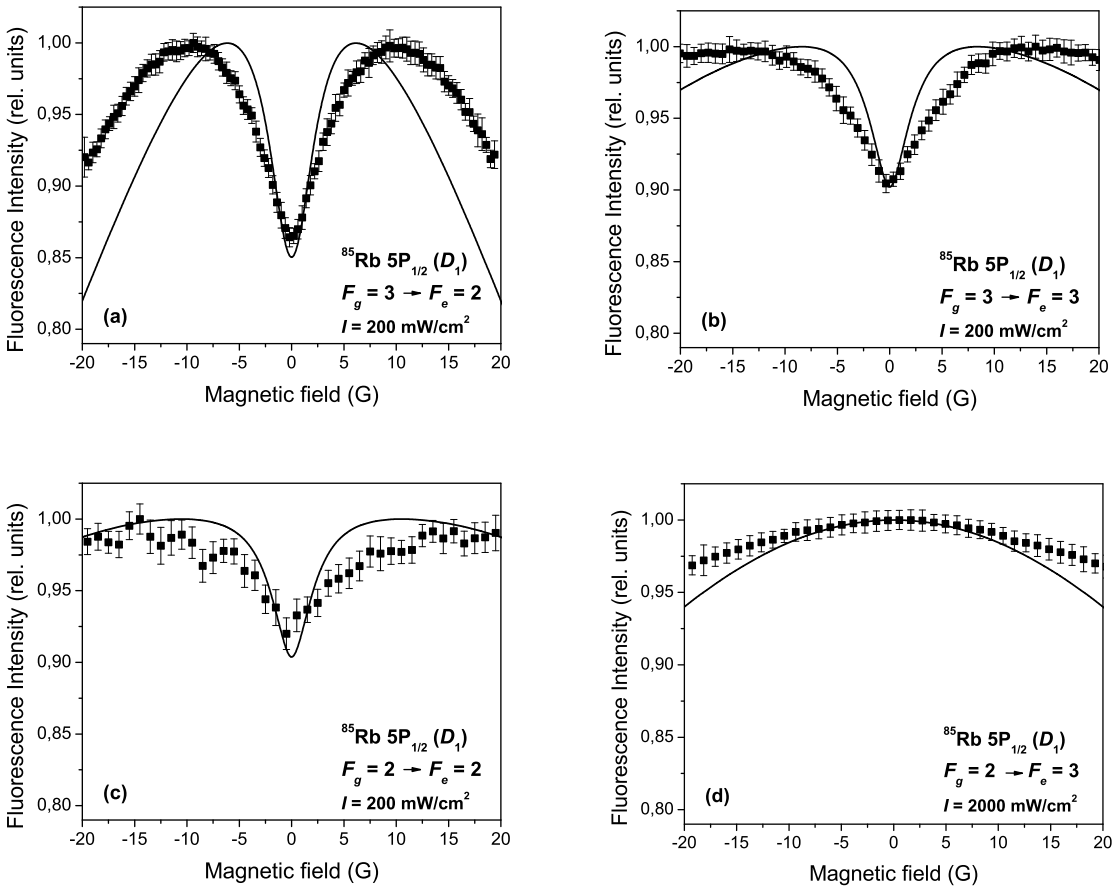

FIG. 6: Fluorescence intensity versus magnetic field for ^{85}Rb at D_1 excitation. Filled squares, experiment; solid line, theory. The excited state, total angular momentum of the ground F_g and excited states F_e of the transition, and laser power density I are given in each panel. $L = \lambda$.

for the transitions with $F_g < F_e$, which was consistent with the theoretical calculations. One of the main differences between these resonances in the ETC and the resonances in an ordinary vapor cell was that resonances in an ETC were substantially broader and had smaller contrast. The experimental signals were described with a theoretical model that was based on the optical Bloch equations that had been previously used to describe successfully these types of resonances in ordinary vapor cells. The model achieved satisfactory agreement in the case of the ETC when values for the model parameters were used that corresponded to the particular characteristics of the ETC. No additional physics processes had to be taken into account in order to describe the experimental signals. The theoretical model suggested that the relaxation rate γ was a key parameter for describing the signals, but that γ in the ETC depended on the ETC wall separation instead of on the laser beam diameter, as in ordinary vapor cells. The best-fit parameters also indicated that the atoms in the ETC had a residual Doppler distribution in the direction perpendicular to the cell walls that was on the order of 60 MHz (FWHM). The results showed that it is possible to describe nonlinear magneto-optical resonances in ordinary cells and ETCs over a wide range of experimental conditions with the same theoretical model, which was based on the optical Bloch equations, and averaged over the Doppler profile, included all neighboring hyperfine transitions, took into account the splitting and mixing of the magnetic sublevels in an external magnetic field, and treated the coherence properties of the radiation field. As a result, theoretical modeling can serve as a reliable tool for future investigations with ETCs and for the development of practical applications based on them. The remaining imperfections in the agreement between

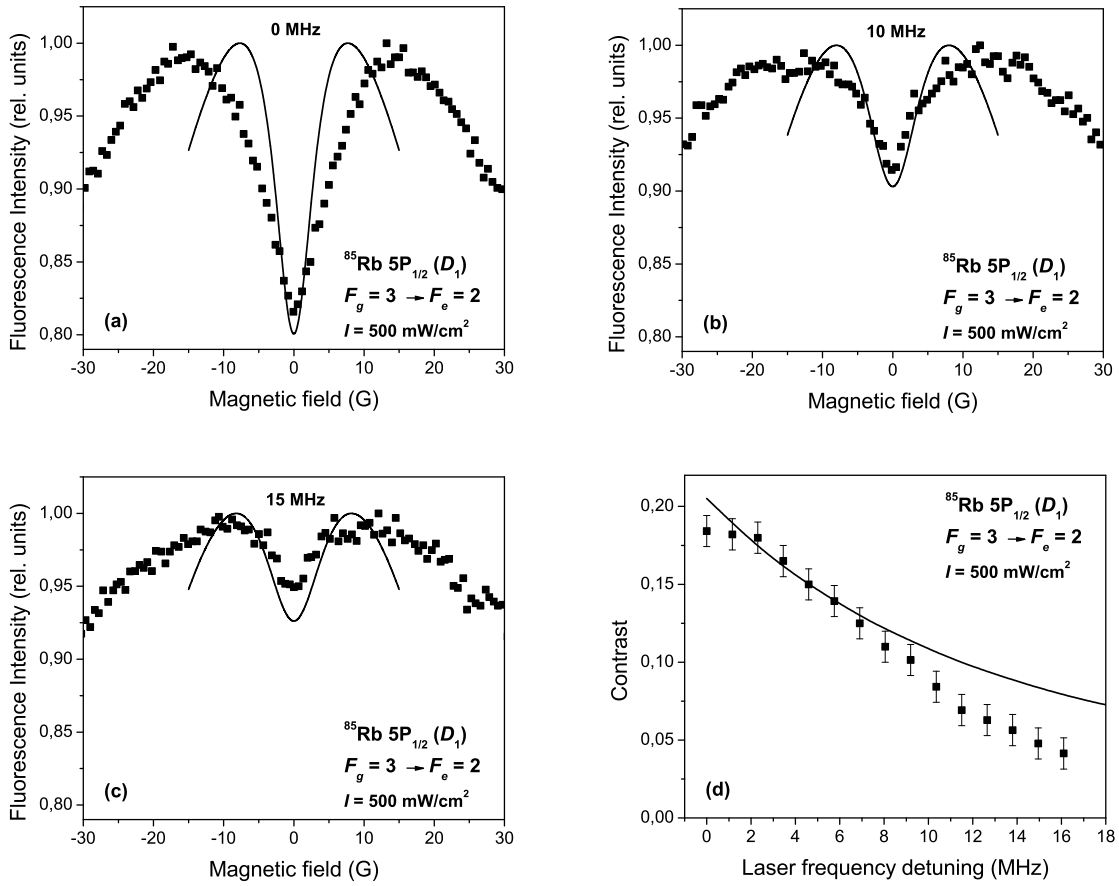

FIG. 7: (a-c) Fluorescence intensity versus magnetic field for the $F_g = 3 \rightarrow F_e = 2$ transition of ^{85}Rb at D_1 excitation at various values of the laser detuning with respect to the exact position of the $F_g = 3 \rightarrow F_e = 2$ transition; (d) resonance contrast versus laser frequency detuning. Filled squares, experiment; solid line, theory. $L = \lambda$.

theory and experiment suggest that there do exist additional physical effects that should be taken into account or treated in greater detail in the theoretical description of the ETC.

Acknowledgments

The Riga group would like to thank Maris Tamanis for assistance with the experiments and Christina Andreeva for useful discussions and to acknowledge support from the Latvian National Research Programme in Material Sciences Grant No. 1-23/50 and the Latvian Science Council Grant No. LZP 09.1196. The work in Ashtarak was supported in part by the INTAS South-Caucasus Grant 06-1000017-9001.

[1] D. Sarkisyan and A. Papoyan, *Optical processes in micro- and nanometric thin cells containing atomic vapor* (Nova Science Publishers, 2009), vol. 263 of *Horizons in World Physics*, chap. 3, pp. 85–124.

[2] A. Sargsyan, G. Hakhumyan, A. Papoyan, D. Sarkisyan, A. Atvars, and M. Auzinsh, Applied Physics Letters **93**,

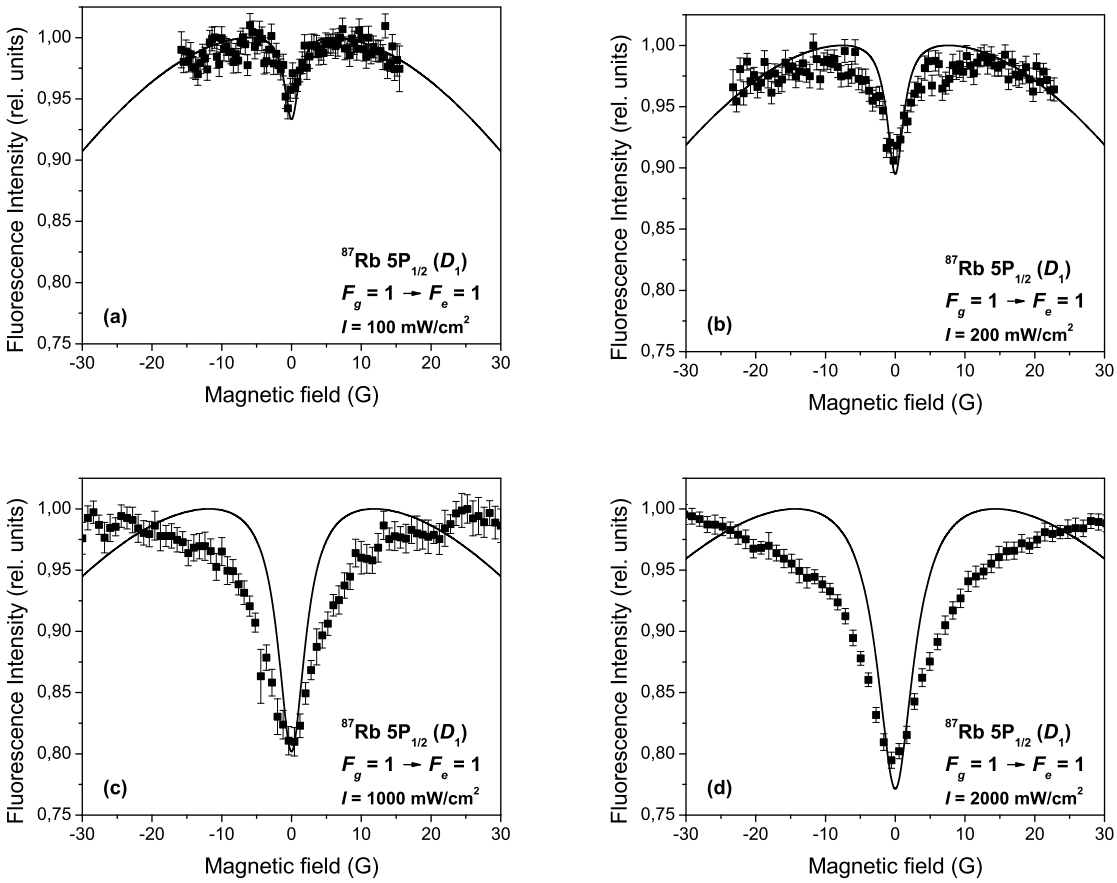

FIG. 8: Resonance signals for ^{87}Rb at the $F_g = 1 \rightarrow F_e = 1$ transition for different laser power densities I. Filled squares, experiment; solid line, theory. $L = \lambda$.

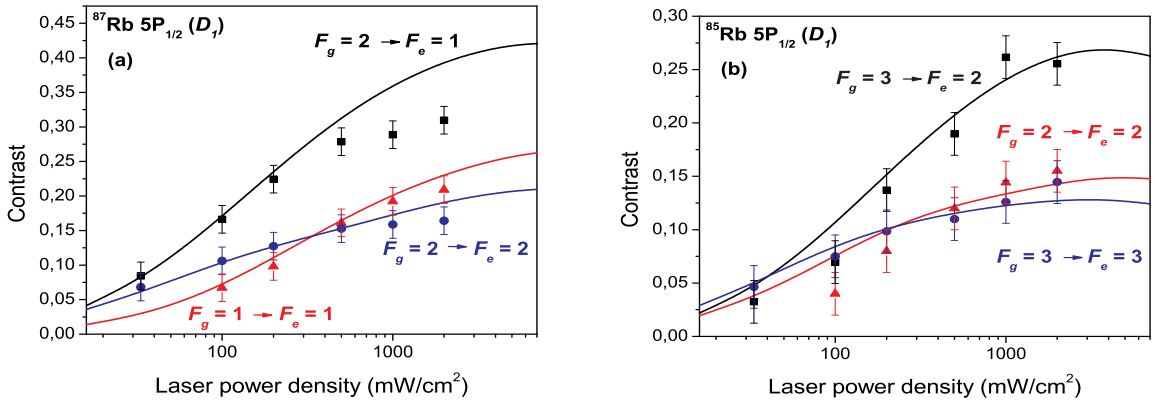

FIG. 9: (color online) Resonance contrast as a function of laser power density for (a) ^{87}Rb and (b) ^{85}Rb dark resonances. Markers, experiment; solid line, theory. $L = \lambda$.

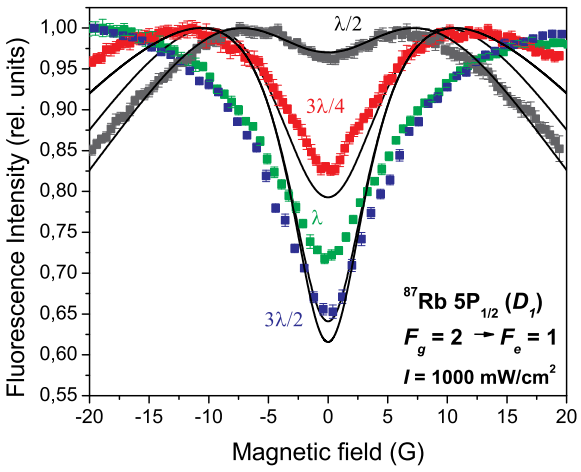

FIG. 10: (color online) Fluorescence intensity versus magnetic field at various values of the wall separation for the $F_g = 2 \rightarrow F_e = 1$ transition of ^{87}Rb. Markers, experiment; solid line, theory.

021119 (2008).
[3] D. Sarkisyan, D. Bloch, A. Papoyan, and M. Ducloy, Optics Communications **200**, 201 (2001).
[4] G. Alzetta, A. Gozzini, L. Moi, and G. Orriols, Il Nuovo Cimento B **36**, 5 (1976).
[5] R. W. Schmieder, A. Lurio, W. Happer, and A. Khadjavi, Physical Review A **2**, 1216 (1970).
[6] Y. Dancheva, G. Alzetta, S. Cartalava, M. Taslakov, and C. Andreeva, Optics Communications **178**, 103 (2000).
[7] C. Andreeva, A. Atvars, M. Auzinsh, K.Bluss, S. Cartaleva, L. Petrov, and D. Slavov, Physical Review A **76**, 063804 (2007).
[8] M. Auzinsh, R. Ferber, F. Gahbauer, A. Jarmola, and L. Kalvans, Physical Review A **78**, 013417 (2008), ISSN 10941622.
[9] M. Auzinsh, R. Ferber, F. Gahbauer, A. Jarmola, and L. Kalvans, Physical Review A **79**, 053404 (2009), ISSN 10941622.
[10] J. C. Lehmann and C. Cohen-Tannoudji, C.R. Acad. Sci. (Paris) **258**, 4463 (1964).
[11] J. L. Picqué, J. Phys. B: Atom. Molec. Phys. **11**, L59 (1978).
[12] A. V. Papoyan, M. Auzinsh, and K. Bergmann., European Physical Journal D **21**, 63 (2002).
[13] K. Blushs and M. Auzinsh, Physical Review A **69**, 063806 (2004).
[14] D. A. Steck, *Rubidium 85 d line data* (2009), (revision 2.1.2, 12 August 2009), URL `http://steck.us/alkalidata`.
[15] D. A. Steck, *Rubidium 87 d line data* (2009), revision 2.1.2, 12 August 2009, URL `http://steck.us/alkalidata`.
[16] C. Andreeva, S. Cartaleva, Y. Dancheva, V. Biancalana, A. Burchianti, C. Marinelli, E. Mariotti, L. Moi, and K. Nasyrov, Physical Review A **66**, 012502 (2002), ISSN 10941622.
[17] S. Stenholm, *Foundations of Laser Spectroscopy* (Dover Publications, Inc., Mineoloa, New York, 2005).
[18] L. Allen and J. H. Eberly, *Optical Resonance and Two Level Atoms* (Wiley, New York, 1975).
[19] N. G. van Kampen, Physics Reports **24**, 171 (1976).
[20] G. Breit and I. I. Rabi, Physical Review **38**, 2082 (1931), ISSN 15366065.
[21] E. B. Aleksandrov, M. Chaika, and G. I. Khvostenko, *Interference of Atomic States* (Springer Verlag, Berlin, 1993).
[22] A. P. Kazantsev, V. S. Smirnov, A. M. Tumaikin, and I. A. Yagofarov, Opt. Spectrosk. (USSR) **57**, 116 (1984).
[23] F. Renzoni, S. Cartaleva, G. Alzetta, and E. Arimondo, Physical Review A **63**, 065401 (2001).
[24] J. Alnis and M. Auzinsh, Physical Review A **63**, 023407 (2001), arXiv:physics/0011050.
[25] A. Sargsyan, D. Sarkisyan, and A. Papoyan, Physical Review A **73**, 033803 (2006).
[26] Y. Pashayan-Leroy, C. Leroy, A. Sargsyan, A. Papoyan, and D. Sarkisyan, J. Opt. Soc. Am. B **24**, 1829 (2007).